Triple-pane Window with Perovskite QD LSC and HIT Solar Cell

Emme Brownell, Kanha Bhatt, Anne Cheng, Federico Cardenas, Joaquin Gomez

Department of Mechanical Engineering, University of Washington

ME 539—Renewable Energy I

December 9, 2025

Abstract. The paper presents an innovative approach to solar energy through building-integrated photovoltaics (BIPV) using zero-dimensional perovskite quantum dot technology in luminescent solar concentrators (LSC). The design features perovskite quantum dots within a triple-pane tempered glass system, which enhances solar energy capture and directs it to high-efficiency Heterojunction with Intrinsic Thin Layer (HIT) solar cells. Simulations confirm the design's effectiveness for urban skyscrapers, while life cycle and economic analyses demonstrate its ecological benefits and commercial viability, highlighting it as a significant advancement in photovoltaic technology.

Contents

1 Introduction

Quantum dot photovoltaic cells are an emerging technology based on semiconductor nanocrystals' distinct optical and electronic properties (6). A single quantum dot represents a single zero-dimensional nanoparticle between 2 and 10 nanometers wide. Colloidal Synthesis and Plasma Synthesis are two methods for producing these nanocrystals, which have size-dependent band gaps, as seen in Figure 1. By adjusting the synthesis parameters, both techniques can create varying-sized dots that change the light absorption and emission properties. The tunable absorption spectrum and the ability for multi-exciton generation (MEG) make this technology appealing for photovoltaic light harvesting (16). A single absorbed photon can generate multiple electron-hole pairs through carrier multiplication, which is highly favorable compared to current photovoltaic cells, which allow only one exciton per high-energy photon. Applying this technology for building-integrated photovoltaics can accelerate the mission toward zero-energy buildings. This field is rapidly growing, and concepts such as transparent and colored photovoltaics are becoming popular.

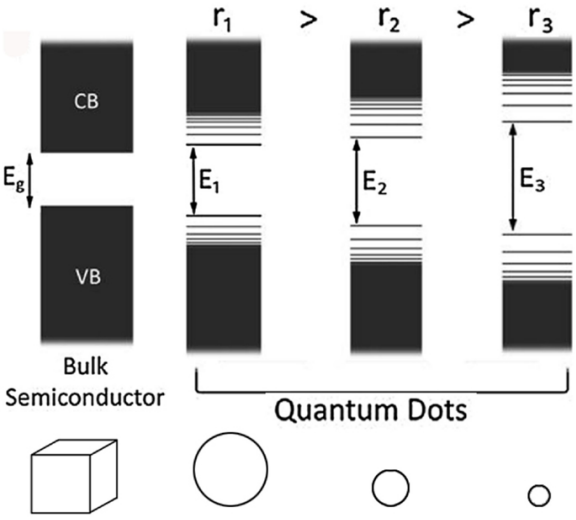

Figure 1: Schematic illustrating levels of semiconductor crystallites with different dimensions (6)

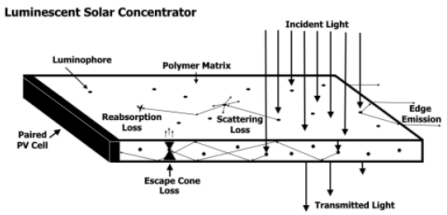

Figure 2: Process of total internal reflection (TIR) within the luminescent solar concentrator (30)

In 2017, a Research group at the Research Center for Renewable Energies and Environment in Italy introduced a design of an LSC Smart Window (3). LSCs are transparent materials such as plastic or glass coated or embedded with fluorescent dyes. The dyes absorb sunlight and re-emit it inside the material. As seen in Figure 2, total internal reflection (TIR) re-emits the lig. It directs it toward the edges of the material, where small solar cells convert it into electricity. Unlike conventional silicon-based solar panels, LSCs can capture direct and diffuse solar radiation, making them practical for cloudy conditions and changing sun orientation. Their design featured four 50 x 50 cm^2 LSC modules incorporated into a double-glazed window; the frame was constructed using thermal break aluminum. The LSC modules were coupled to small silicon solar cells mounted on the edges, and the electricity generated was stored in batteries. Figure 3 shows the innovative window prototype, which generated 12.99 Wh of energy on a clear day in April 2017; the absorbed energy (control system and motors) was approximately 2.66 Wh. Figure 4 illustrates how the components of the yellow smart window fit together to create a solar energy collector.

Figure 3: LSC Smart window prototype installed as fanlights in the paper "Design and performance monitoring of a LSC Smart Window" (3)

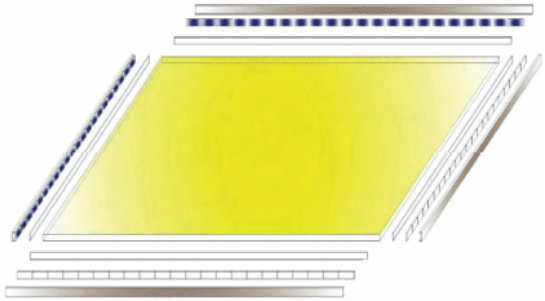

Figure 4: LSC plate with strips of crystalline solar cells on the edges (3)

In 2022, the American Chemical Society (ACS) Photonics journal published a paper regarding Large-Area Transparent "Quantum Dot Glass" (TQDG) for Building-Integrated Photovoltaics (12). Figure 5 shows that the group used silicon quantum dots (Si QDs) embedded in a polymer composite sandwiched between glass layers. The silicon quantum dot material was chosen because of its nontoxicity, abundance, significant Stokes shift, and high photoluminescence quantum yield (PLQY) in the near-infrared (NIR) region. The large-area (400 cm^2) quantum dot glass achieved an overall power conversion efficiency of 1.57% with a back-reflector, contributing to a light utilization efficiency (LUE) of 1.3%. They reported that this was among the top reported performers for transparent photovoltaics using a luminescent solar concentrator [Huang]. Figure 6 represents the Current-voltage (I-V) characteristics of the transparent quantum dot glass under three conditions: intrinsic (standard measurement), unblocked direct illumination, and with a back-reflector. The back-reflector significantly enhances current and power output, improving light trapping and device performance.

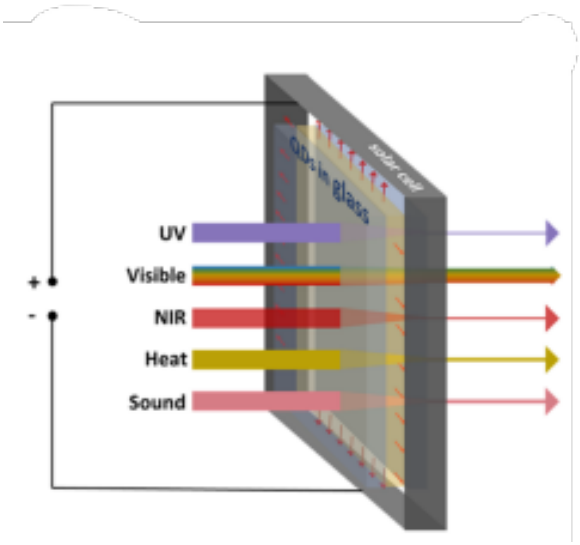

Figure 5: Illustration of the transparent "quantum dot glass" concept (12)

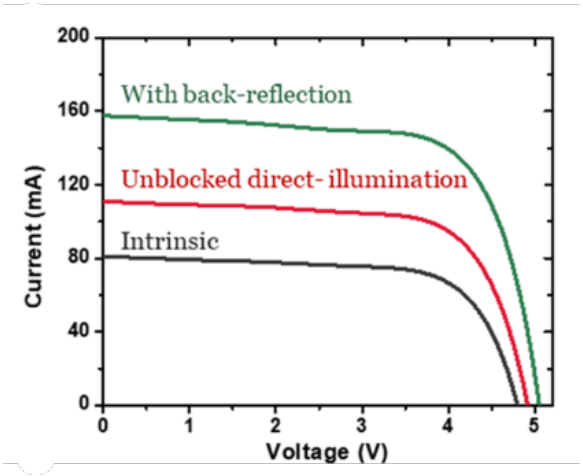

Figure 6: IV curves of transparent quantum dot glass under three lighting conditions (12)

The primary challenges of designing building-integrated photovoltaics are the efficiency vs. transparency tradeoffs, material stability, aesthetic integration, and scaling costs. High transparency will reduce light absorption, leading to lower

efficiency. In contrast, increasing efficiency requires reducing transparency, which may not be desired for architectural applications. Many high-efficiency materials, such as Copper Indium Gallium Selenide (CIGS) and Cadmium QDs, could degrade over time, which limits their suitability for long-term building integration. Additionally, the high cost and complexity of large-area fabrication and low aesthetics with intense color tints will limit large-scale commercialization.

Extensive research has been conducted on Perovskite Quantum Dots Solar Cells (PQDCS) for Building Integrated Photovoltaics (BIPV). PQDCS is highlighted as a promising alternative due to its flexibility, lightweight, color transparency, and high conversion efficiency (19). In an ideal BIPV system, the photovoltaic conversion materials should have a high light absorption coefficient to achieve high efficiency, device structure, and bandgap that can be adjusted, substantial flexibility to meet various needs, mechanical ability to resist compression and bending, the ability for large-scale production, and low cost that is economically suitable for use. Perovskite is highly efficient, with the current laboratory-certified efficiency reaching up to 26.1% (19). It also allows for color adjustability, which can be tuned to match the architectural design requirements. Moreover, perovskite offers lower material costs and multiple preparation methods, which make it economically viable for production.

Several key design constraints exist for Building Integrated Photovoltaics (BIPV). Solar windows must seamlessly integrate into a building's architecture while meeting high load-bearing requirements. Currently, thin film and silicon solar cells are strong candidates for BIPV applications, but there is limited room for improvement in terms of cost, efficiency, and color options (19).

Perovskite quantum dots have emerged as a more promising alternative than thin films or dyes, primarily due to their low cost, enhanced stability, and improved tunability. These metal halides can be classified as either inorganic or organic-inorganic, and they possess optoelectronic properties that make them suitable as emitters in luminescent solar concentrators (LSCs). In particular, zero-dimensional perovskite quantum dots exhibit minimal absorption and emission spectral overlap, a higher photoluminescence quantum yield, robust stability, and simple synthesis (4).

However, much remains to be researched regarding the optimal nanocrystal structure of perovskite quantum dots, and this aspect is still a subject of debate. Researchers are actively exploring the best doping methods and strategies to reduce toxicity, essential for the widespread application of LSCs. While the development of perovskite quantum dots makes this project more hypothetical than traditional thin films, the innovation potential adds an exciting dimension to the research.

This paper unveils an innovative approach to building-integrated photovoltaics (BIPV) solar cells, highlighting a groundbreaking design known as the Perovskite Quantum Dot Window. This window employs sophisticated waveguiding technology to efficiently channel sunlight to solar cells strategically positioned along its edges. Inspired by a pioneering product from UbiQD, the design involves a captivating layering process, where vibrant quantum dots are sandwiched between two sheets of glass. As illustrated in Figure 7, these nanoparticles are engineered to capture sunlight, maximizing the window's energy-harvesting potential. They internalize and refract infrared light, directing it towards the edges where solar cells are located, thus transforming light into electricity with impressive efficacy (24).

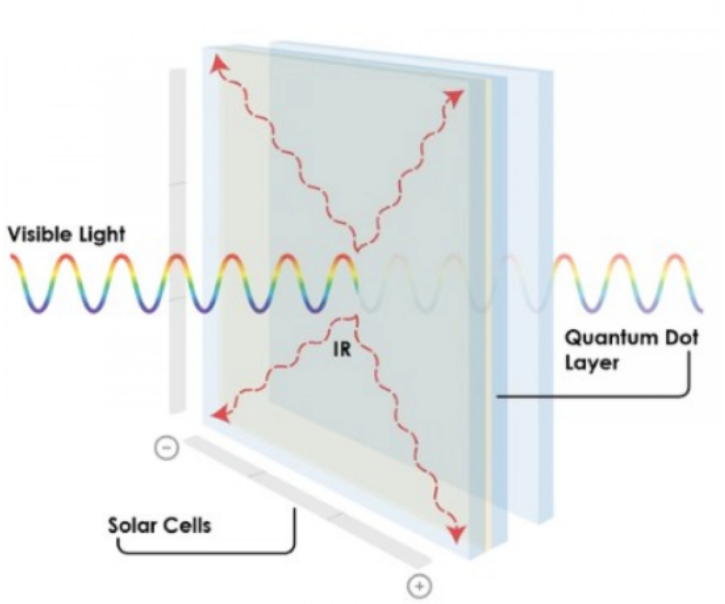

Figure 7: Image illustrating UbiQD's design of an LSC quantum dot "Wendow" with solar cells along the edges (24).

2 Device Design

The window will consist of three layers of high-transparency glass with a space in between. In the sandwiched space between the glass will be the noble gas Argon to prevent decomposition of the quantum dots and provide thermal insulation. A thin layer of a Perovskite Quantum Dot Luminescent Solar Concentrator (LSC) will be applied to the middle glass structure. The LSC will absorb infrared and ultraviolet light and waveguide it to the edges. Heterojunction with Intrinsic Thin Layer (HIT) solar cells will be installed along the edge of the middle window and absorb the re-emitted light. A microinverter will be used for every two window modules to convert DC to AC power individually, ensuring optimal system voltage for maximum peak power voltage and preventing losses from shadowing. The entire window will be 0.61 x 0.61 meters with a thickness of 30 mm. The glass structure will be a high transparency tempered glass with a thickness per pane of 5 mm. The Noble Gas-Filled Gap will be 13 mm thick, and the LSC-Quantum Dot Layer will be 2 mm thick. The solar cells will be placed along all four edges of the window, and each strip will have a width of 0.6 mm. Figure 8 shows a sketch of this proposed design.

The heterojunction structure with intrinsic thin-layer (HIT) Solar Cell is an amorphous and crystalline silicon with an ultra-thin layer of intrinsic a-Si:H inserted between them. The TCO layer was selected to be Indium Tin Oxide (ITO). This material was chosen because of its high optical transmittance and low electrical resistivity. After the ITO, the structure of the cell consists of a-Si:H on both the p+ layer (10 nm) and the intrinsic layer (5 nm). The heterojunction layer is made up of an n-type crystalline Si with a thickness of 200 um. The back contact will be an Aluminum structure deposited using thermal evaporation. Microelectronic industries widely use p-type c-Si wafers for device fabrication, and their mass production presents lower costs than n-type c-Si. As a result, this would help obtain lower-cost HJ and HIT cells (7). The structure of the proposed HIT solar cell can be seen in Figure 13. A solar simulation was executed to understand the performance of this system. AFORS-HET is a numerical simulation tool used for modeling homo- and heterojunction devices. It solves one-dimensional semiconductor equations based on Shockley–Read–Hall recombination statistics (25).

The results in this section are an AFORS-HET simulation carried out by the Department of Physics at Mulawarman University in Indonesia. The simulation was conducted at a stable temperature of 300K with an Air Mass Coefficient of 1.5 AM (26). Table 1 displays some of the input values used in the simulation study. Figure 12 displays the fill factor and efficiency values in the varying TCO work functions and dopant concentrations. The Work Function (WF) represents the minimum energy required to remove an electron from a material's surface into the vacuum. It represents the energy barrier that electrons must overcome to escape from the material. An optimal WF for the TCO (with Ohmic-like contact) will prevent the formation of a Schottky barrier and allow for stable carrier transport. The figure shows that a Fill Factor of 75% and an Efficiency of 25% can be achieved with a higher WF TCO and a dopant concentration of 5.0 x 10^{19}. Figure 11 represents the IV Curve with varying Work Functions for the TCO layer ranging from 4.9 to 5.2 eV. The chart shows that a value of 5.2 eV outputs an open circuit voltage of 634.2 mV and a short circuit current of 51.2 $\frac{\text{mA}}{\text{cm}^2}$. The declining trends display how different WF TCO values significantly impact peak-level performance for solar cell output (26). A wide range of open-circuit voltages and a narrow range of short-circuit voltages can be seen in the graph. An energy band diagram using a high dopant concentration of 5.0 x 10^{19} can be seen in Figure 9. The chart displays that a WF TCO value from 5.2

to 5.6 eV outputs a smooth band transition with a step-like junction at the interfaces of the materials.

Parameter	(p)a-Si:H	(i)a-Si:H	a-Si:H/c-Si interface	(n)c-Si
Thickness (nm)	10	5	-	2×10^{3}
Dielectric constant	11.9	11.9	-	11.9
Electron affinity (eV)	3.9	3.9	-	4.05
Band gap (eV)	1.8	1.72	-	1.124
Effective cond. band density (cm^{-3})	2.5×10^{20}	2.5×10^{20}	-	2.846×10^{19}
Effective val. band density (cm^{-3})	1.0×10^{19}	2.5×10^{20}	-	2.685×10^{19}
Acceptor concentration, Na (cm^{-3})	5.0×10^{16}	0	-	0
Donor concentration, Nd (cm^{-3})	0	0	-	1.5×10^{16}
Electron mobility ($cm^{2} \cdot V^{-1} \cdot s^{-1}$)	20	20	-	1111
Hole mobility ($cm^{2} \cdot V^{-1} \cdot s^{-1}$)	5	5	-	421.6
Electron thermal velocity ($cm \cdot s^{-1}$)	1.0×10^{7}	1.0×10^{7}	-	1.0×10^{7}

Table 1: The input values used in the simulation study by the Department of Physics at Mulawarman University (26)

In amorphous silicon solar cells, a large part of recombination is *bulk recombination*, which occurs in the center of the intrinsic layer due to the dangling bonds acting as recombination centers (27). A lower defect density value indicates that the semiconductor fabrication and deposition were satisfactory. Figure 10 shows the defect density variations versus Fill Factor and Efficiency for two WF TCO values. A 2016 study found that the dopant concentration value should be double the defect density (Ntr) rate (9). The figure shows a higher efficiency and fill factor at lower defect densities. The final proposed design of this ITO / (p+)a-Si: H / (i)a-Si: H / (n)c-Si / Al solar cell structure shows a maximum theoretical efficiency of 23.67%. The results and parameters of this simulation can be seen in Table 2.

2.1 Materials & Methods

Materials:

Parameter	Value	Unit
Maximum Efficiency	23.67	%
Open-Circuit Voltage (VOC)	634.2	mV
Short-Circuit Current Density (JSC)	51.2	mA/cm^2
Fill Factor (FF)	72.91	%
Work Function of TCO (WFTCO)	5.2	eV
Emitter Doping (Na)	5.0×10^{19}	cm^{-3}
Base Doping (N)	1.0×10^{18}	cm^{-3}
Interface Defect Density (Dit)	1.0×10^{10}	cm^{-3}

Table 2: The results and parameters of the simulation in the 2016 study by Ghannam (9)

- Polymer Matrix for LSC
  - Polymethyl Methacrylate (PMMA)
- Perovskite QD luminophore for LSC
  - oD Cs 4Pb(Br)6 QD
- Noble gas
- Tempered glass
  - Anti-reflective coating
- Heterojunction with Intrinsic Thin Layer (HIT) Solar Cell

Manufacturing:

- Spray coating
  - changed to roll-to-roll coating after further consideration and research done in Section 4.

2.2 Diagrams & Sketches

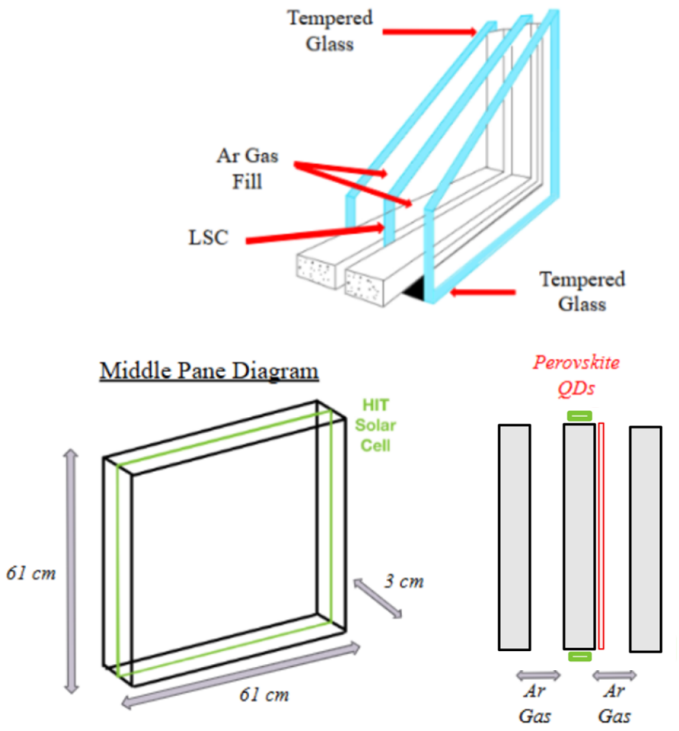

Figure 8: Proposed design sketch of triple-pane perovskite QD LSC window with HIT solar cells

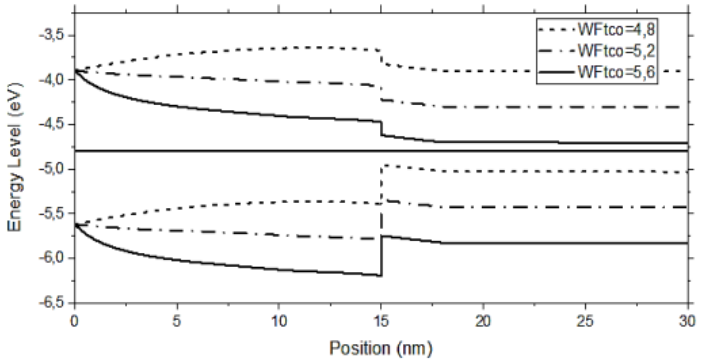

Figure 9: Band diagram (26)

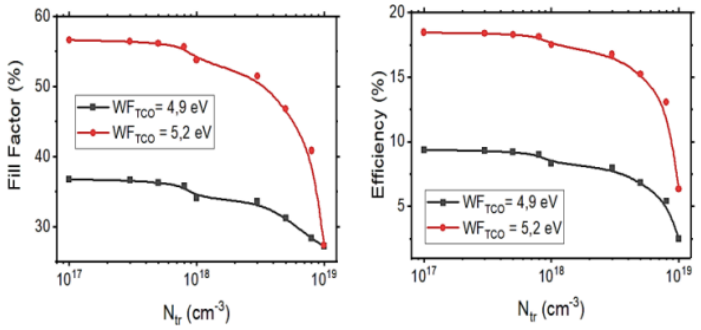

Figure 10: Defect density (26)

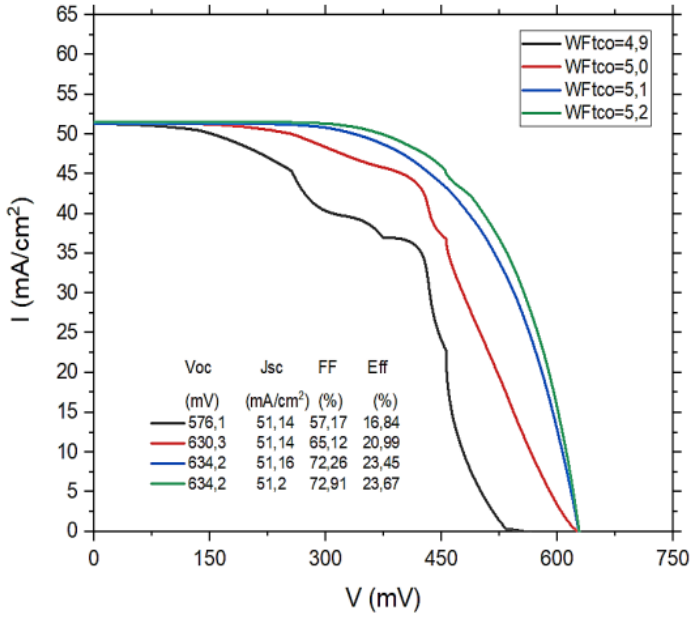

Figure 11: HIT Cell IV Curve (26)

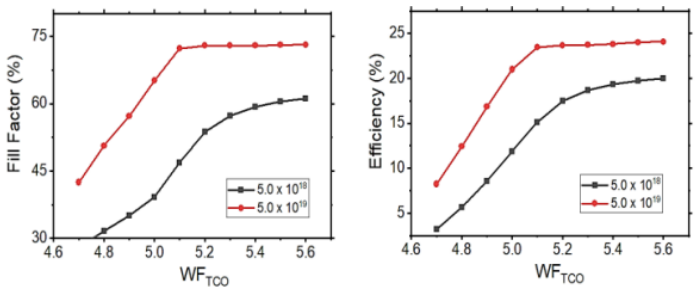

Figure 12: Fill Factor Efficiency (26)

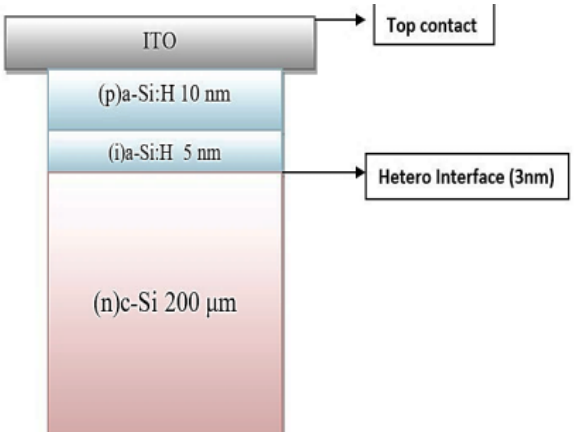

Figure 13: HIT Cell Structure (26)

3 System Design

The most significant appeal of luminescent solar concentrators is not their efficiency, as by all accounts, standard monocrystalline silicon boasts a greater efficiency, but its advantage in maintaining a building's aesthetics and functionality. For urban skyscrapers, with buildings so often designed with more windows than is practically necessary, LSC built into these pre-existing structures or included in the plans for a new one can optimize these locations for solar harvesting. Another fact to consider is that in some places where there is undoubtedly enough sun for effective PV systems, it is too hot for silicon-based PV systems to operate at their optimal efficiencies. Such a factor can make owners of these towering buildings hesitant to invest in silicon. Although CdTe modules tolerate intense temperatures, the price point is much higher. LSC presents an option that is both cheaper (as much as can be surmised) and isn't limited to the surface area of the roof, lest mounted modules get positioned on the walls of the building, which is not only a safety hazard to those on the streets but compromises the aesthetics of the structure.

The location chosen for the site of installation of the solar modules plays a role in deciding the parameters on which to base the design. The Chase Tower in Phoenix is 483 feet and 40 stories tall (a picture of the building can be seen in figure 14)(5). The windows alternate between rectangular and square shapes on the upper floors, where the solar modules would operate at their best performance due to the lack of shading from surrounding buildings. The optimal areas to install the windows in the building would be the west- and east-facing sides. The north end was ruled out due to the suboptimal sunlight, as Phoenix, Arizona, is within the Northern Hemisphere. The southern-facing facade was also deemed suboptimal due to its construction, which would cause it to be shaded by its own shadow; for ease of simulation, it was excluded from consideration.

Figure 14: Image of the Chase Tower in Pheonix Arizona (5)

Most studies on LSCs contain experimental results that use square sections as the substrate on which the quantum dots are embedded or coated. To best use these results effectively, the area of the chosen windows should also be square, which is permitted under the limitations of the selected location. This flexibility is why, as seen in section 2, the area of the LSC measured was chosen to be 2 ft x 2 ft, or 0.61 m x 0.61 m. Each tower floor on the western and eastern facades has 14 windows, with those floors closest to the top being the most optimal for LSC installation due to the more significant amount of sun exposure.

3.1 Simulation & Modeling

The parameters detailed in section 2 and introduced at the beginning of section 3 lay the essential groundwork for crafting simulated plots and diagrams that genuinely capture the intricacies of relevant data. Drawing from the assumptions regarding the orientation of the panels concerning the azimuth, alongside the strategic positioning of the building and its dimensions—height and width—a sophisticated shading model was meticulously developed. This model serves to illuminate how the building's shading impacts the efficiency and power output of the solar modules.

Undertaking this analysis is particularly complex due to the multitude of variables that can influence shading dynamics, becoming even more pronounced when assessing the luminescent solar concentrators (LSCs) placed on a facade that languishes in shadow for half a day. The results of this intricate simulation, unveiling the interplay of light and shade, can be found in section 3.3. Meanwhile, the calculations designed to identify the most effective variables for enhancing the performance of the PV module are detailed in section 3.2.

3.2 Calculations for Module Performance & Efficiency

To accurately simulate the performance of the photovoltaic system, it is essential first to assess an individual module's efficiency and power output. This assessment must consider the interactions between the luminescent solar concentrator (LSC) and the high-efficiency HIT cells positioned along the edges of the waveguiding material. Understanding these dynamics will reveal the true potential of the system's performance.

LSC and HIT Cell Performance Equations:

1. LSC External Optical Efficiency (30)

$$\eta_{opt} = \frac{P_{out} \times A_{edge}}{P_{in} \times A_{LSC}} = \frac{P_{out}}{P_{in} \times G} \tag{1}$$

where

- I = solar irradiance constant (1000 W/m^2),
- η_{opt} = 2.4% (0.024) under the one-sun condition in the 2019 study by Zhao et al. (30),
- A_{LSC} = the area of the window

$$A_{LSC} = 0.61m \times 0.61m = 0.3721m^2$$

- A_{edge} = A rea of the edges of the window.

$$A_{edge} = 0.61\text{m} \times 0.006\text{m} \times 4 \text{ sides} = 0.01454\text{m}^2$$

- P_{in} = incident optical power on the window (372.1 W)

$$P_{in} = I \times A_{LSC},$$

- G = geometric factor accounting for the device design (25.42),

$$G = \frac{A_{LSC}}{A_{edge}}$$

- P_{out} = optical power emerging at the LSC edges.

$$P_{out,\,ideal} = \eta_{opt} \times P_{in} \times G = 226.981 \text{ W}$$

However, due to reabsorption, scattering, and coupling loss, only a fraction of the ideal reaches the photovoltaic cells (30),(4). A true representation of the power as an effective experimental value is:

$$P_{edge,\,in} = \eta_{opt} \times P_{in} = 8.904 \text{ W}$$

2. Overall LSC-HIT cell PV Efficiency (System Efficiency) (4):

$$\eta_{system} = \eta_{opt} \times \eta_{PV} = \frac{P_{elec,\,out}}{P_{in}} \tag{2}$$

where

- η_{PV} = HIT cells conversion efficiency
- η_{system} = overall electrical efficiency. According to the papers "Zero-Dimensional Perovskite Nanocrystals for Efficient Luminescent Solar Concentrators" and "Luminescence solar concentrators: A technology update," perovskite LCEs have a power conversion efficiency of approximately 1.8%(0.018) (30),(4).
- $P_{elec,\,out}$ = electrical power output by the LSC

$$P_{elec,\,out} = \eta_{system} \times P_{in} = 6.6978 \text{ W}$$

3. HIT Cell Short-Circuit Current Density (4):

$$J_{SC} = q \int_{\lambda_{min}}^{\lambda_{max}} \phi_{edge}(\lambda)\, EQE(\lambda)\, d\lambda \tag{3}$$

where

- q is the elementary charge (1.6×10^{-19} C),
- $\phi_{edge}(\lambda)$ = photon flux density at the LSC edge ($\frac{\mu mol}{m^2 s}$),
- $EQE(\lambda)$ = external quantum efficiency of the HIT cell,
- λ_{min} and λ_{max} = wavelength limits of the cell's spectral response.

4. HIT Cell Diode Equation (I-V Characteristic) (4):

$$J(V) = J_0 \left(\exp\left(\frac{qV}{nkT} \right) - 1 \right) - J_{SC} \tag{4}$$

where

- J_0 = reverse saturation current density (A/m^2),
- V = the voltage across the cell (V),
- n = the ideality factor,
- k = Boltzmann's constant (1.38×10^{-23} J/K),
- T = the absolute temperature (K).

5. Open-Circuit Voltage (4):

$$V_{OC} = \frac{nkT}{q} \ln\left(\frac{J_{SC}}{J_0} + 1 \right) \tag{5}$$

6. Fill Factor (FF) and Maximum Power Point (MPP) (4):

$$FF = \frac{J_{mp} V_{mp}}{J_{SC} V_{OC}} \tag{6}$$

$$P_{max} = J_{mp} \times V_{mp} \times A_{cell} \tag{7}$$

where

- J_{mp} and V_{mp} = current density at the maximum power point,
- V_{mp} = voltage at the maximum power point,
- A_{cell} = effective area of the HIT cell.

Several variables in these equations cannot be estimated without using difficult-to-learn theoretical models and ray-tracing simulations or by experiments on a prototype. However, other variables have already been determined in comprehensive studies. η_{opt}, for example, was determined to be as high as 2.4% under one sun illumination according to the 2019 paper "Zero-Dimensional Perovskite Nanocrystals for Efficient Luminescent Solar Concentrators" (30).

Other variables need to be estimated as no studies were found that directly tested zero-dimensional perovskite LSC with amorphous silicon heterojunction with thin, intrinsic layer cells. Therefore, to properly simulate the device's function within the system design, it is necessary to guess parameters to the best of one's ability. A list of these parameters are:

- The open-circuit voltage (V_{OC}) was approximated to be about 0.6 volts per HIT cell, making one window (module) have an estimated V_{OC} of 28.8 volts.
- The maximum power point voltage (V_{MP}) is typically 80% of the V_{OC}, thus it was estimated to be 23 volts.
- The maximum power point current (I_{MP}) is calculated using Ohm's Law:

$$I_{MP} = \frac{P_{elec,\,out}}{V_{MP}} = 0.29 \text{ A}$$

- The short-circuit current (I_{SC}) can be approximated by multiplying the cell area by the short-circuit current density (J_{SC}), which relies on the photon flux density at the edge of the LSC ($\phi_{edge}(\lambda)$) and the external quantum efficiency of the HIT cell (EQE(λ)). $\phi_{edge}(\lambda)$ can only be measured with a spectroradiometer or estimated from calibrated optical measurements. Thus, it cannot be calculated and only estimated. Since the cells of the module are all in series, it can be assumed that the I_{SC} is greater than the I_{MP}, and it is estimated to be 0.32 A.

Two variables must be adjusted to test the module in SAM. The maximum power point and short-circuit current were calculated using a cell area of 0.0144 m^2, below SAM's minimum requirement of 0.05 m^2 for active areas. Therefore, even though the power and efficiency would be calculated without issue (as seen in Figure 15), the I-V curve and system simulation would fail to solve for the normalized coefficients. To address this issue, the parameters were scaled up to meet the minimum by assuming multiple identical HIT cells are connected in parallel. As a result of this scaling, the expected output power of the module was modified to 23.3 volts, and the expected efficiency was adjusted to 6.26%, as can be seen in 16. Consequently, the final maximum power point current I_{MP} was determined to be 1.01 amps, and the final short-circuit current I_{SC} was 1.11 amps.

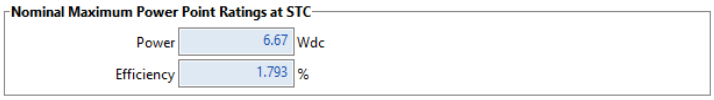

Figure 15: Ratings at standard testing conditions before scaling for SAM Simulation.

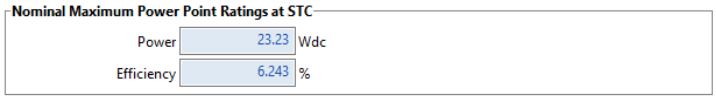

Figure 16: Ratings at standard testing conditions after scaling for SAM Simulation

To accurately simulate the combined performance of the luminescent solar concentrator and HIT solar cells, the CEC Performance Model with user-entered specifications was employed to ensure that all necessary variables were accounted for. The input variables are:

1. Maximum power point voltage (Vmp): 23 V
2. Maximum power point current (Imp): 1.01 A
3. Open circuit voltage (Voc): 28.8 V
4. Short circuit current (Isc): 1.11 A

5. Temperature coefficient of Voc: -0.26 $\frac{\%}{^\circ C}$
6. Temperature coefficient of Isc: 0.05 $\frac{\%}{^\circ C}$
7. Temperature coefficient of max. power-point: -0.2 $\frac{\%}{^\circ C}$
8. Number of cells in series: 48
9. Nominal operating cell temperature: 46 °C
10. Module area: 0.3721 m^2
11. Module aspect ratio: 1.000

The temperature coefficients were estimated based on informed assumptions derived from comparisons of different silicon-based solar cells. These three variables are particularly susceptible to inaccuracies because, unlike other variables that can be calculated or theorized based on research data, the temperature coefficients are not discussed in any studies. Instead, they can only be inferred from commercial data, which is often unreliable and not directly applicable to this scenario.

3.3 Results

The system design simulation was done through the National Renewable Energy Laboratory (NREL) System Advisor Model. The specifications for the module found in research papers are calculated using known variables or estimated based on what information has been acquired. The current-voltage curve at standard testing conditions for the

The horizon (or sun-path) diagrams that were generated using the program PVsyst version 8.0.7 (shown in Figure 17 show little to no difference between the amount of time modules on the west side of the building are exposed to direct sunlight compared to the modules installed on the eastern facade. Therefore, when specifying the azimuth of the windows, a general 90 degrees for westwards facing was all that was measured as the sun paths allow one to assume that the results would be similar enough to draw the same conclusion regardless.

When running the NREL SAM simulation, three different variations of the western facade were tested: 2 modules with optimal placement at the top windows of the tower, 14 modules consisting of the highest floor of the tower, and 56 modules consisting of the highest four floors, with each two modules having one inverter. The figures generated in the simulation summary can be found in the Appendix A. The current-voltage characteristics for the module (IV-curves) can be seen in figure 18.

With two modules and one inverter:

- Annual AC energy in year 1: 15 kWh
- DC capacity factor in year 1: 3.8%
- Energy yield in year 1: 330 kWh/kW
- Performance ratio in year 1: 0.28
- Shading Losses: -18.912%
- Module deviation from STC: -61.63%
- Figure 24: represents the alternating current energy collected annually for every month.

- Figure 25: represents the alternating current energy collected annually for everyday.

With 14 modules and seven inverters (one row of windows):

- Annual AC energy in year 1: 106 kWh
- DC capacity factor in year 1: 3.7%
- Energy yield in year 1: 327 kWh/kW
- Performance ratio in year 1: 0.27
- Shading Losses: -20.26%
- Module deviation from STC: -61.30%
- Figure 26: represents the alternating current energy collected annually for every month.
- Figure 27: represents the alternating current energy collected annually for every day.

With 56 modules and 28 inverters (four rows of windows):

- Annual AC energy in year 1: 365 kWh
- DC capacity factor in year 1: 3.2%
- Energy yield in year 1: 281 kWh/kW
- Performance ratio in year 1: 0.23
- Shading Losses: -61.27%
- Module deviation from STC: -31.39%
- Figure 28: represents the alternating current energy collected annually for every month.
- Figure 29: represents the alternating current energy collected annually for every day.

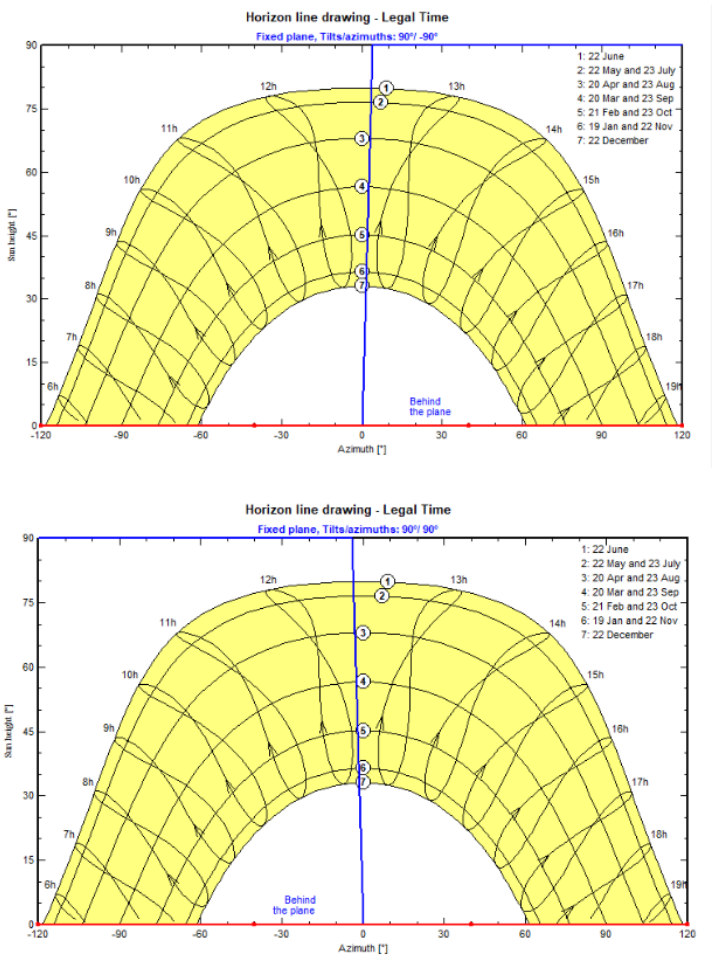

Figure 17: Horizon diagrams of the eastern facade (top diagram) and the western facade (bottom diagram).

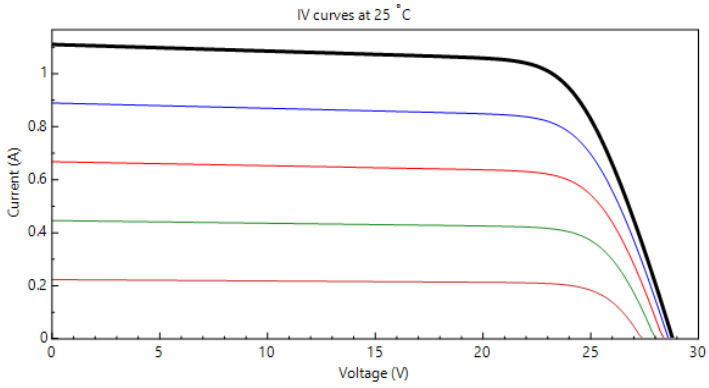

Figure 18: SAM NREL generated IV curves of the LSC and HIT solar cells working as a single module (Black: $1000\frac{W}{m^2}$, Blue: $800\frac{W}{m^2}$, Orange: $600\frac{W}{m^2}$, Green: $400\frac{W}{m^2}$, and Red: $200\frac{W}{m^2}$).

4 Manufacturing Plan

This manufacturing plan outlines the production process for an innovative building-integrated photovoltaic (BIPV) window system. The system incorporates a triple-pane tempered glass design with a luminescent solar concentrator (LSC) based on perovskite quantum dots (QDs) and high-efficiency heterojunction with intrinsic thin-layer (HIT) silicon solar cells. The goal is to deliver scalable, aesthetically integrated, and energy-generating windows suitable for high-rise commercial buildings.

The BIPV window assembly includes the following major components:

1. Triple-pane tempered glass (61 cm × 61 cm)
2. Perovskite QD Luminescent Solar Concentrator (LSC)
3. HIT Solar Cells (a-Si/c-Si)
4. Microinverters (e.g., Enphase IQ 8D)
5. Argon gas fills

The manufacturing process is divided into the stages (pictured in figure 19):

Figure 19: Manufacturing workflow for perovskite QD BIPV Windows

1. **Glass Preparation**

   In this initial stage, tempered glass panels are cut to the designated size (61 cm × 61 cm), and the edges are polished for safety and aesthetics. At this step, any necessary openings or grooves for wiring are machined. Cleanroom-grade washing and drying are recommended to remove particulate contaminants that could interfere with coating adhesion in later stages.

2. **Quantum Dot Coating**

   A perovskite quantum dot (QD) solution is prepared and deposited onto the inner surface of the middle glass pane. The coating process can utilize spin-coating for uniform thin films or spray-coating for scalable production. The coated pane is then cured under controlled conditions (e.g., inert argon atmosphere and low temperature) to prevent oxidation and degradation of the QD layer.

3. **Solar Cell Integration**

   HIT (heterojunction with intrinsic thin-layer) solar cells are aligned and mounted along the edges of the coated middle pane. This edge-mounting ensures the efficient collection of waveguided photons from the LSC. Electrical interconnections between cells are formed using conductive adhesives or soldering, and insulation layers are applied as needed to prevent shorts.

4. **Window Assembly**

   The outer, middle (QD-coated), and inner panes are assembled into a sealed triple-glass unit. Inert argon gas is injected between the panes to improve thermal insulation and enhance the longevity of the QD materials. A transparent encapsulant or polymer spacer ensures proper alignment and sealing, preventing moisture ingress.

5. **Electrical System Integration**

   The final step involves connecting the edge-mounted HIT cells to external circuitry and microinverters. Wiring is routed along concealed channels in the window frame for aesthetics and safety. A junction box or DC combiner may be added depending on the system scale. Each window or window pair is connected to a microinverter for grid-tied power delivery.

4.1 Cost Calculations

Assume the equipment lifespan is 5 years, depreciation per window is:

$$\frac{400,000}{5 \times 12 \times 36,000} = 0.19$$

Assume there are 10 workers, $4000 per month each, cost per window is:

$$\frac{10 \times 4,000}{3,600} = 1.11$$

Assume $0.12 kWh, and 5 kWh per window, cost per window is:

$$\frac{36,000 \times 5 \times 0.12}{36,000} = 0.6$$

Material	Cost (USD per window)
Tempered Glass	$30
Quantum Dot Coating	$15
HIT Solar Cell	$25
Sealant	$5
Wiring & Electrical Parts	$10
Argon Gas Fill	$3
Total Material Cost	**$88**

Equipment	Cost (USD)
Quantum Dot Coating Machine (Spin/Spray)	$200,000
HIT Solar Cell Encapsulation Machine	$150,000
Argon Gas Filling System	$50,000
Total Equipment Investment	**$400,000**

Figure 20: Cost breakdown PV window production

Other parameter assumptions:

- Production rate: 50 windows/hr

- Operating time: 24 hr/day, 30 days, a month
- Total monthly production: 36000 windows/ month

After running all these calculations, it can be inferred that the approximate total cost per window is USD 89.9.

4.2 Economics of Scale

As production volume increases, the cost per BIPV window significantly decreases due to economies of scale. Fixed costs, such as equipment investment, are spread across more units, while bulk material purchasing and improved process efficiency further reduce per-unit costs. For example, increasing output from 10,000 to 100,000 units per month lowers the cost per window from $80 to $62. Additional savings can be achieved through material optimization, energy-efficient processing, and semi-automated assembly. These reductions make technology more economically viable for large-scale implementation in commercial buildings.

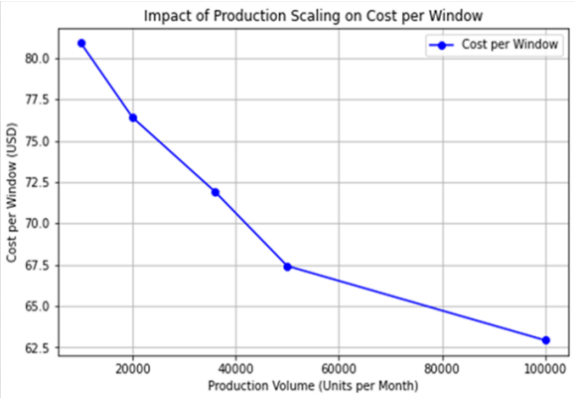

Figure 21: Impact of production scaling on the cost per window

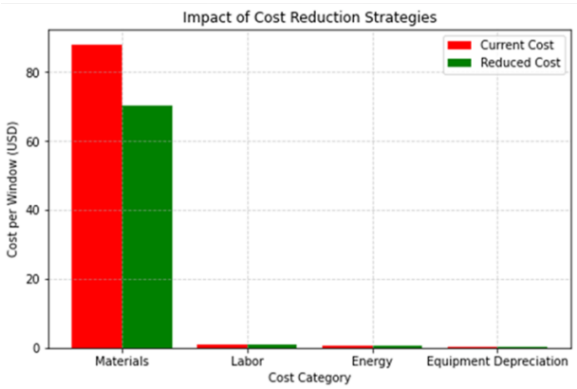

Figure 22: Impact of economics of scale cost reduction strategies

4.3 Technical Challenges and Risk Assessment

1. **Stability of Perovskite Quantum Dots (PQDs)**: Perovskite Quantum Dots are remarkably sensitive entities, easily affected by moisture, oxygen, and the relentless onslaught of ultraviolet radiation. These environmental factors can accelerate their degradation, leading to decreased device performance over time, as highlighted in studies (16).
2. **Complexity in Manufacturing**: Creating a flawless and uniform coating of PQDs on expansive glass surfaces presents a daunting challenge. Achieving this level of perfection is crucial for maintaining high quality and performance standards (28).
3. **Interface Engineering**: To facilitate optimal energy transfer between the Luminescent Solar Concentrator (LSC) and Heterojunction Intrinsic Thin-Layer (HIT) solar cells, meticulous attention is required in engineering the interfaces. Each layer must be precisely tailored for maximum efficiency.
4. **Long-term Reliability**: Photovoltaic-integrated windows are designed to withstand the rigors of various weather conditions. Their ability to maintain peak performance in changing climates is essential for long-term reliability, ensuring they remain practical and durable over time (3).

4.4 Sustainability Analysis

1. **Material Considerations**: A significant number of photonic quantum devices (PQDs) are composed of lead, which raises urgent environmental concerns due to its toxic nature and potential harm to ecosystems and human health (17).
2. **Energy Efficiency Contribution**: These innovative windows allow natural light to pour in while maintaining their clarity and harness solar energy, generating electricity. This dual functionality aligns seamlessly with the principles of sustainable architecture, promoting a harmonious balance between nature and human design.
3. **Life Cycle Assessment (LCA)**: The life cycle assessment reveals a stark reality: while glass production contributes considerably to global warming potential (GWP), the synthesis of PQDs is associated with even higher levels of ecotoxicity and negative health impacts (11), highlighting the pressing need for careful consideration and innovative approaches in materials science.

4.5 Future Improvement Suggestions

1. **Material Innovation**: Focus on creating and optimizing lead-free perovskite materials to enhance photovoltaic device performance while significantly minimizing environmental toxicity associated with traditional lead-based compounds. This initiative aims to ensure a greener approach to solar technology without compromising efficiency.
2. **Process Optimization**: Implement advanced, scalable coating techniques such as spray-coating and inkjet printing. These methods allow for the precise application of thin films on various substrates, offering cost-effectiveness and high-throughput manufacturing processes, ensuring consistent quality and performance across large-scale production runs (28).
3. **Advanced Encapsulation**: Develop innovative encapsulation methods utilizing multilayer barrier technologies or Atomic Layer Deposition (ALD). These approaches enhance the durability and lifespan of Photovoltaic Quantum Dot (PQD) devices by providing superior protection against environmental factors such as moisture and oxygen, prolonging operational efficiency, and reducing degradation over time.
4. **System Integration Enhancements**: Seamlessly integrate PQD technology with innovative grid systems and advanced monitoring solutions. This integration facilitates real-time performance tracking, enables better energy management, and improves overall system responsiveness, allowing for optimized operation in varying environmental conditions and enhancing the adaptability of renewable energy sources.

5 Life Cycle Analysis (LCA)

The window that is being proposed is composed of both perovskite solar cells and quantum dot luminescent layers. The LCA assessments of the perovskite PV modules are done to determine the overall sustainability from raw material extraction and manufacturing through to operation and end-of-life management. The production of these PQD windows begins with synthesizing the perovskite quantum dots, which involve specific solvents and materials that influence the environmental footprint of PQDs. The National Renewable Energy Laboratory (NREL) reported that these material-intensive processes and energy consumption are major contributors to the ecological footprint (22). Lately, lower-toxicity solvents, materials, and methods have been improved, such as solvent recycling and opting to use copper and other less toxic materials. Manufacturing of the PQD windows can be very energy-demanding and inefficient (17). More efficient and less energy-demanding manufacturing techniques are being developed and show a promising reduction in the footprint of these devices (17). Recycling can help reuse valuable materials, solvents, etc, to reduce the environmental impact. When in operation, perovskite PV modules have shown to have a 24% cumulative energy demand (CED) reduction for installed systems (17).

5.1 Goal & Scope

This Life Cycle Assessment (LCA) for perovskite quantum dot (PQD) windows is designed to meticulously evaluate the environmental impact across every stage of their life cycle. This analysis delves deep into the journey from acquiring raw materials to the intricate manufacturing processes, the operation efficiency, and the considerations for end-of-life disposal or recycling. The LCA aims to draw a vivid comparison between the ecological footprints of conventional photovoltaic (PV) systems and our innovative PQD windows. By harnessing a blend of cutting-edge technologies, these windows enhance energy efficiency, optimize material usage, and minimize overall emissions, promising a more sustainable future.

5.2 Inventory Analysis

Understanding the intricacies of the raw materials and their procurement for perovskite quantum dot (PQD) windows is pivotal in assessing their environmental impact and overall life cycle. The primary components employed in perovskite systems consist of various solvents and chemicals, most notably dimethylformamide (DMF) and octadecene (ODE). According to the National Renewable Energy Laboratory (NREL), the energy expenditure required for synthesizing precursors can account for a considerable 15-25% of the total energy inputs. This noteworthy statistic emphasizes the importance of energy efficiency in this process (16).

Manufacturing these innovative cells involves intricate steps, including film deposition, precise laser patterning, and protective encapsulation. Historically, these procedures have demanded significant amounts of energy. However, recent findings from the NREL indicate a promising shift, showcasing a remarkable reduction in manufacturing energy consumption by approximately 20% (22).

Regarding operational performance, PQD-based solar cells are still on the path to maximizing their power con-

version efficiency (PCE) when juxtaposed with traditional photovoltaic (PV) systems. Nevertheless, the evolution of PQD technology has been nothing short of transformative, propelling their PCE from a modest 3.8% to an impressive 20.1% over the years (16). This upward trajectory highlights the potential for innovation in renewable energy and the exciting future for sustainable energy solutions.

5.3 Impact Assessment

The main impact from this installation has been normalized to global warming potential (GWP), which has been approximated in kg CO_2 equivalencies. Other impact categories will also be mentioned in this assessment. The initial analysis shows that the tempered glass used in the window has the highest GWP impact (Figure 23). The production step of the glass accounts for the highest emissions due to the high temperatures required for glass manufacturing (1). Additionally, the quantity of glass utilized for the window installation, estimated at 510 $\frac{kg}{m^2}$, contributes significantly to the overall impact.

Other categories where glass from the windows has a notable influence include the release of toxic gases like NOx and SO_2, as well as particulate matter, dramatically affecting the Fine Particulate Matter Formation category and human carcinogenic toxicity levels. Transportation of the glass from Michigan to the site in Arizona also results in substantial emissions. One potential method to offset the glass's environmental impact is recycling. However, the challenge lies in the necessity to remelt the glass for recycling, which accounts for over 80% of all emissions associated with glass production (1).

The second category with the highest impact was the LSC, which had a GWP of 400 kg CO_2-eq. This impact primarily stemmed from the matrix used to contain the quantum dot, as it was relatively large compared to the rest of the installation. Other significant impacts from the LSC included freshwater ecotoxicity, human carcinogen and non-carcinogen toxicity, and mineral resource scarcity. Heavy metals contributed most significantly to all these categories, while the solution process utilized to create the quantum dots was a significant factor in freshwater ecotoxicity. Proper recycling of materials could substantially reduce the toxicity associated with this process. The transportation of the LSC from China to Arizona had a relatively low impact, which allowed for the grouping of shipping with that of the HIT solar cell, resulting in emissions of 3.39 kg CO_2-eq due to the low shipping weight.

The section with the lowest impact was the HIT solar cell. Despite its relatively high impact compared to other components, the cell's small size required a limited amount of material for the installation.

5.4 Interpretation

The information utilized to perform this Life Cycle Assessment (LCA) was obtained through OpenLCA software, along with additional papers for data unavailable in the database. The database information is from 2018 and is specific to Europe. Data related to glass processing was also sourced from Europe and published by a glass manufacturing company, which may introduce a bias. The emissions associated with the Life Cycle Stage (LSC) processing of Quantum Dots (QDs) could not be located, resulting in their exclusion from the LCA.

Initial emissions were calculated for the High-Intensity Transition (HIT) solar cell section using data from a paper (10) that claimed no vested interest in the published information. This paper included emissions for producing metallurgical grade silicon, accounting for various suppliers and production locations. The worst-case scenario for low-quality silica mined and processed in China was selected for this assessment.

Information regarding Indium Tin Oxide (ITO) emissions and recycling was gathered from three different papers (14; 2; 29), which also indicated no bias and sourced their research from various global locations. An approximation for the Energy Payback Time (EPBT) calculation was made based on emissions to produce an equivalent amount of electric power in Phoenix, AZ, using data from the EPA's Greenhouse Gas Equivalencies Calculator. Transportation emissions were calculated using a software tool provided by a German NGO that calculates shipping emissions based on cargo weight and shipping method.

Certain elements, including the inverter and the argon gas used between the panels, were omitted from the LCA due to a lack of readily available information. Recyclability was considered in the final LCA. As the building would have required new windows during the renovation regardless, the impact of the glass was excluded from the EPBT calculations. The EPBT for this installation is estimated to be 2 years and 10 months.

Cell and module parts	**GWP (kgCo2-eq)**
HIT Solar Cell	0.32547
LSC	399.582
Tempered Glass	8262
Total window GWP	8661.907
Transportation China-Arizona	3.390
Transportation Michigan-Arizona	88.690
Total GWP	8753.987
Total emissions without glass	403.297
Embodied energy (-glass; kWh)	1085.000

Figure 23: Global warming potential of each material and form of transport involved in upstream process

6 Conclusion

Developing and implementing a Perovskite Quantum Dot-based Luminescent Solar Concentrator represents a significant leap forward in sustainable and efficient building-integrated photovoltaics. The proposed system mitigates conventional issues such as reabsorption losses and limited transparency by capitalizing on the unique optical properties and high photoluminescence quantum yield of zero-dimensional Cs4PbBr6 perovskite nanocrystals. Simulations performed using the NREL System Advisor Model illustrate substantial efficiency gains, especially when strategically deployed on urban high-rise structures' east- and west-facing facades. However, there is also something to be said about choosing a building with a side facing the equator that is actually usable for maximum solar power exposure. Evaluating the western facade, however, not only allows for reasonable extrapolation of the results to the eastern facade but is a model that can extend to buildings centered on the equator where the northern and southern faces of the buildings aren't receiving more sun than the other and thus receiving similar amounts of shadowing.

Although the results are promising, the design and commercialization of this innovative system encounter several technical and environmental challenges. One major issue is the material stability, particularly the sensitivity of perovskite quantum dots to moisture and oxygen. This requires advanced encapsulation techniques and careful selection of protective materials. Additionally, there are environmental concerns related to lead-based perovskites, which highlight the need for accelerated research into sustainable, lead-free alternatives to ensure broader acceptance and compliance with regulatory standards. Furthermore, there is the inconclusiveity of the simulation tests due to the limitations of the System Advisor Model. To truly determine the feasibility of the triple-paned, perovskite quantum dot LSC with HIT solar cells, it is necessary to do more in depth simulation with more sophisticated software and testing with a possible prototype.

Nevertheless, continuous advancements in materials science and scalable manufacturing processes are essential to fully realize the potential of perovskite quantum dot solar technology. By improving durability, cost-efficiency, and environmental impact, this innovative photovoltaic solution has significant promise for widespread integration into modern architecture. It can greatly contribute to global renewable energy goals and support the sustainable development of future urban landscapes. Further testing would tell whether perovskite quantum dots have a future in LSC technology at the brink of so much photovoltaic innovation.

References

[1] AGC Glass Europe. (n.d.). *Environmental impact of flat glass production*. AGC Glass Europe. https://www.agc-glass.eu/en/sustainability/decarbonisation/environmental-impact

[2] Arvidsson, R., Kushnir, D., Molander, S., & Sandén, B. A. (2016). Energy and resource use assessment of graphene as a substitute for indium tin oxide in transparent electrodes. *Journal of Cleaner Production*, **132**, 289–297. https://www.sciencedirect.com/science/article/pii/S0959652615004515?via%3Dihub

[3] Aste, N., Del Pero, C., Buzzetti, M., Fusco, R., Testa, D., Leonforte, F., & Adhikari, R. S. (2017). Design and performance monitoring of a LSC Smart Window. *2017 6th International Conference on Clean Electrical Power (ICCEP)*, 179–183. https://ieeexplore.ieee.org/document/8004812

[4] Castelletto, S., & Boretti, A. (2023). Luminescence solar concentrators: A technology update. *Nano Energy*, **109**, 108269. https://www.sciencedirect.com/science/article/pii/S2211285523001052?via%3Dihub

[5] Council on Tall Buildings and Urban Habitat. (n.d.). Chase Tower - the skyscraper center. https://www.skyscrapercenter.com/phoenix/chase-tower/8894

[6] Dong, G., Wang, H., Chen, G., Pan, Q., & Qiu, J. (2015). Quantum dot-doped glasses and fibers: Fabrication and optical properties. In Y. Yue (Ed.), *Frontiers in Materials*, **2**, 1–14. https://www.frontiersin.org/journals/materials/articles/10.3389/fmats.2015.00013/full.

[7] Dwivedi, N., Kumar, S., Bisht, A., Patel, K., & Sudhakar, S. (2013). Simulation approach for optimization of device structure and thickness of hit solar cells to achieve ~ 27% efficiency. *Solar Energy*, **88**, 31–41. https://www.sciencedirect.com/science/article/pii/S0038092X12003994

[8] European Commission. (2023, June). *Nodes containing EF data*. European Platform on LCA | EPLCA. https://eplca.jrc.ec.europa.eu/LCDN/contactListEF.html

[9] Ghannam, M., Abdulraheem, Y., & Shehada, G. (2016). Interpretation of silicon degradation hit solar cells due to inadequate front contact TCO work function. *Solar Energy Materials and Solar Cells*, **145**, 423–431. https://www.sciencedirect.com/science/article/abs/pii/S0927024815005632?via%3Dihub

[10] Heidari, S. M., & Anctil, A. (2022). Country-specific carbon footprint and cumulative energy demand of metallurgical grade silicon production for silicon photovoltaics. *Resources, Conservation and Recycling*, **180**, 106171. https://www.sciencedirect.com/science/article/abs/pii/S0921344922000192

[11] Hsu, D. D., O'Donoughue, P., Fthenakis, V., Heath, G. A., Kim, H. C., Sawyer, P., Choi, J., & Turney, D. E. (2012). Life Cycle Greenhouse Gas Emissions of Crystalline Silicon Photovoltaic Electricity Generation. *Journal of Industrial Ecology*, **16**(S1), 122–135. https://onlinelibrary.wiley.com/doi/10.1111/j.1530-9290.2011.00439.x.

[12] Huang, J., Zhou, J., Jungstedt, E., Samanta, A., Linnros, J., Berglund, L. A., & Sychugov, I. (2022). Large-Area Transparent "Quantum Dot Glass" for Building Integrated Photovoltaics. *ACS Photonics*, **9**(7), 2499–2509. https://pubs.acs.org/doi/10.1021/acsphotonics.2c00633.

[13] IEA. (2022). *Executive summary – solar PV global supply chains – analysis*. IEA. https://www.iea.org/reports/solar-pv-global-supply-chains/executive-summary

[14] Kedara Shivasharma, T., Sahu, R., Rath, M. C., Keny, S. J., & Sankapal, B. R. (2023). Exploring tin oxide based materials: A critical review on synthesis, characterizations and supercapacitive energy storage. *Chemical Engineering Journal*, **477**, 147191. https://www.sciencedirect.com/science/article/pii/S1385894723059223

[15] Kim, A., Hosseinmardi, A., Annamalai, P. K., Kumar, P., & Patel, R. (2021, May 24). Review on colloidal quantum dots luminescent solar concentrators. *Chemistry Europe*. https://chemistry-europe.onlinelibrary.wiley.com/doi/abs/10.1002/slct.202100674.

[16] Kim, M. R., & Ma, D. (2015). Quantum-dot-based solar cells: Recent advances, strategies, and challenges. *The Journal of Physical Chemistry Letters*, **6**(1), 85–99. https://doi.org/10.1021/jz502227h.

[17] Leccisi, E., Lorenz, A., & Fthenakis, V. (2023). Life-Cycle Analysis of Crystalline-Si "Direct Wafer" and Tandem Perovskite PV Modules and Systems. *IEEE Journal of Photovoltaics*, **13**(1), 16–21. https://doi.org/10.1109/jphotov.2022.3220958.

[18] Li, H., Zeng, X. B., Xie, X. B., Yang, P., Li, J. Y., Zhang, X. D., & Wang, Q. M. (2013). The Amorphous/Crystalline Silicon Interface Research of HIT Solar Cells by Simulation. *Advanced Materials Research*, **773**, 124–131. https://doi.org/10.4028/www.scientific.net/amr.773.124.

[19] Li, Z., Wu, H., & Wang, R. (2024). Actuality and technology prospect of using perovskite quantum dot solar cells as the photovoltaic roof. *Solar Energy*, **269**, 112359. https://doi.org/10.1016/j.solener.2024.112359.

[20] Maalouf, A., Okoroafor, T., Jehl, Z., Babu, V., & Resalati, S. (2023). A comprehensive review on life cycle assessment of commercial and emerging thin-film solar cell systems. *Renewable and Sustainable Energy Reviews*, **186**, 113652. https://www.sciencedirect.com/science/article/pii/S1364032123005099

[21] Mahmud, M. A., & Farjana, S. H. (2020). Comparative eco-profiles of Polyethylene Terephthalate (PET) and polymethyl methacrylate (PMMA) using life cycle assessment. *Journal of Polymers and the Environment*, **29**(2), 418–428. https://link.springer.com/article/10.1007/s10924-020-01885-7#citeas

[22] National Renewable Energy Laboratory. (2012, November). Life Cycle Greenhouse Gas Emissions from Solar Photovoltaics. NREL. https://www.nrel.gov/docs/fy13osti/56487.pdf.

[23] National Renewable Energy Laboratory. (2024, March). Energy and Carbon Payback Times for Modern U.S. Utility Photovoltaic Systems. NREL. https://www.nrel.gov/docs/fy24osti/88653.pdf.

[24] Paleja, A. (2022, November 5). Transparent solar panels will soon become a window of energy and light in your home. UbiQD. https://ubiqd.com/2022/11/05/transparent-solar-panels-will-soon-become-a-window-of-energy-and-light-in-your-home/.

[25] Rawat, A., Sharma, M., Chaudhary, D., Sudhakar, S., & Kumar, S. (2014). Numerical simulations for high efficiency HIT solar cells using microcrystalline silicon as emitter and back surface field (BSF) layers. *Solar Energy*, **110**, 691–703. https://www.sciencedirect.com/science/article/pii/S0038092X14004903

[26] Satriani, I. L., Munir, R., Natalisanto, A. I., & Hamdani, D. (2023). Analysis of ITO/a-Si:H(p)/a-Si:H(i)/c-Si(n)/Al HIT (Heterostructure with Intrinsic Thin Layer) solar cell performances. *ELKHA*, **15**(1), 11–17. https://www.researchgate.net/publication/370110525_Analysis_of_ITOa-SiHpa-SiHic-SinAl_HIT_Heterostructure_with_Intrinsic_Thin_Layer_solar_cell_performances

[27] Shah, A. (2012). Chapter IC-1 - Thin-Film Silicon Solar Cells. In A. J. McEvoy, T. Markvart, & L. Castañer (Eds.), *Practical Handbook of Photovoltaics: Fundamentals and Applications* (2nd ed., pp. 209–281). chapter, Elsevier, Academic Press. Retrieved March 6, 2025, from https://www.sciencedirect.com/science/article/abs/pii/B9780123859341000088.

[28] Wang, J., Yuan, Y., Schneider, J., Zhou, W., Zhu, H., Cai, T., & Chen, O. (2022). Quantum Dot-based Luminescent Solar Concentrators Fabricated through the Ultrasonic Spray-Coating Method. *ACS Applied Materials & Interfaces*, **14**(36), 41013–41021. https://pubs.acs.org/doi/10.1021/acsami.2c11205.

[29] Xu, W., Chen, X., Liu, D., Jiang, W., & Yang, B. (2023). Systematic thermodynamic and experimental studies for recovering indium and tin from indium tin oxide waste target with hydrogen. *Journal of Cleaner Production*, **429**, 139328. https://www.sciencedirect.com/science/article/pii/S0959652623034868

[30] Zhao, H., Sun, R., Wang, Z., Fu, K., Hu, X., & Zhang, Y. (2019). Zero-Dimensional Perovskite Nanocrystals for Efficient Luminescent Solar Concentrators. *Advanced Functional Materials*, **29**(30). https://advanced.onlinelibrary.wiley.com/doi/10.1002/adfm.201902262.

A Appendix

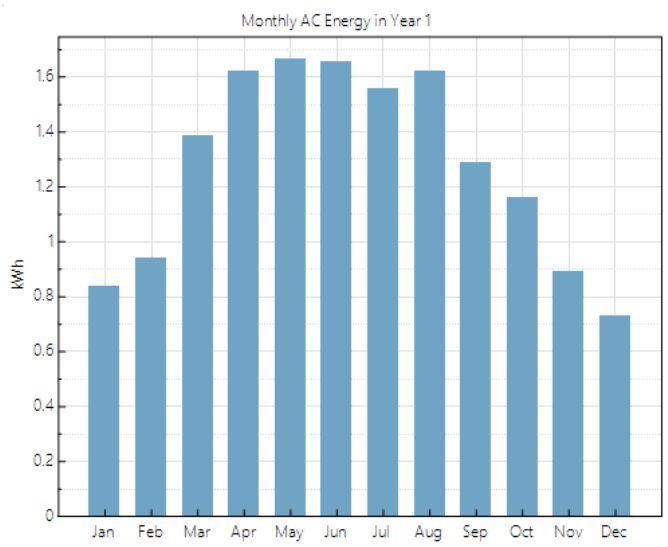

Figure 24: AC energy collected during the 1st year of operation for each month (for two modules)

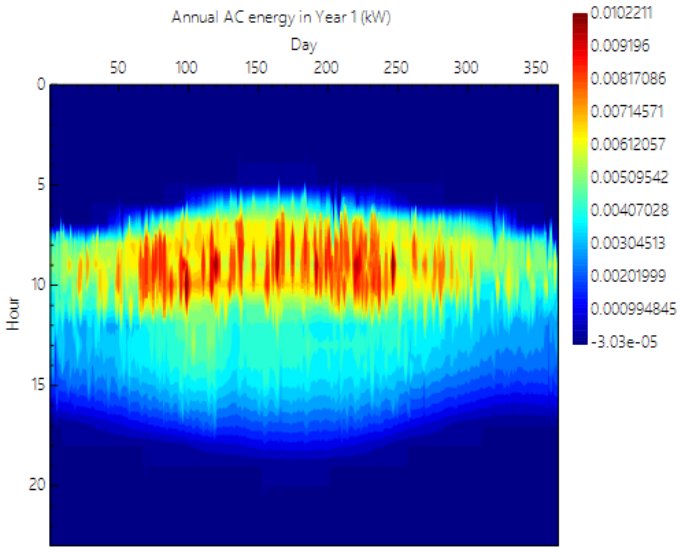

Figure 25: AC energy collected during the 1st year of operation for each day (for two modules)

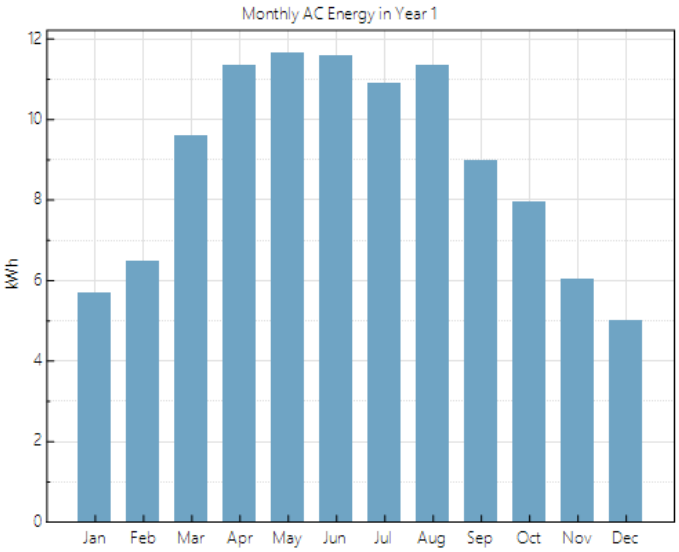

Figure 26: AC energy collected during the 1st year of operation for each month (for 14 modules)

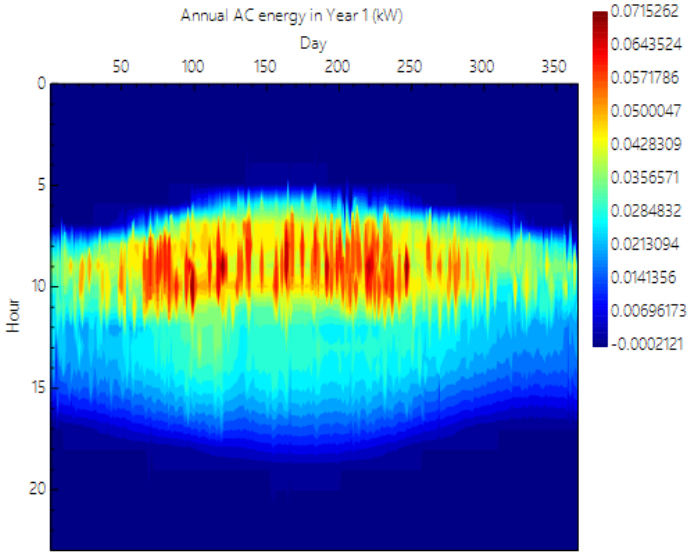

Figure 27: AC energy collected during the 1st year of operation for each day (for 14 modules)

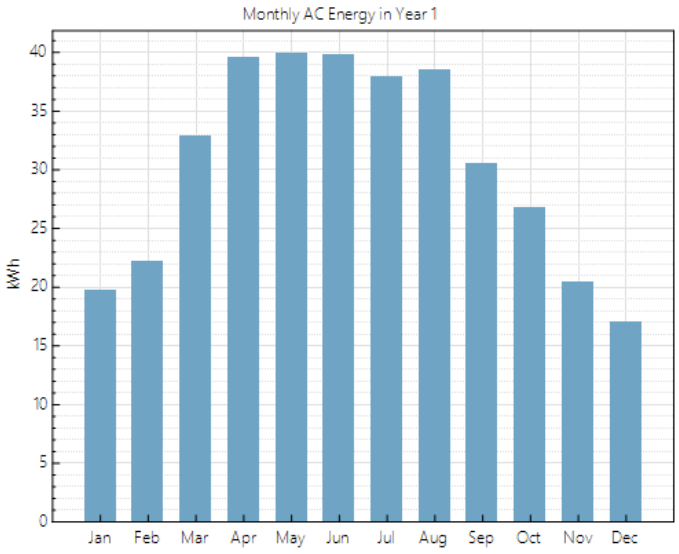

Figure 28: AC energy collected during the 1st year of operation for each month (for 56 modules)

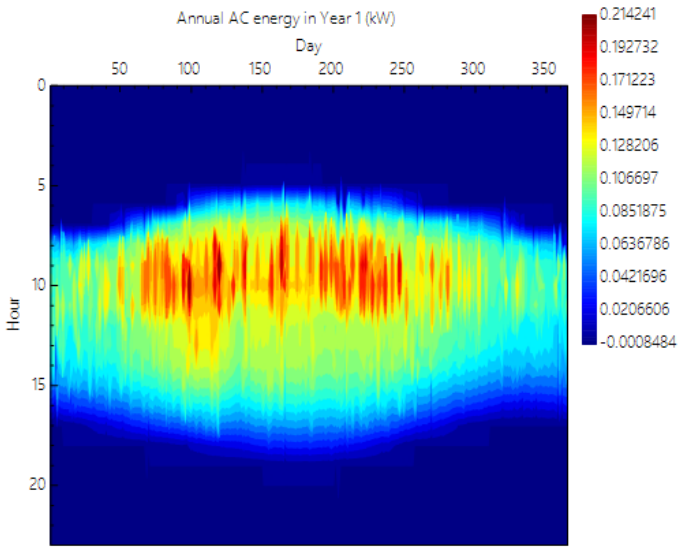

Figure 29: AC energy collected during the 1st year of operation for each day (for 56 modules)